Condensation nuclei measurements in the midlatitude (1982–2012) and Antarctic (1986–2010) stratosphere between 20 and 35 km

Patrick Campbell[1] and Terry Deshler[1]

Received 19 February 2013; revised 27 November 2013; accepted 2 December 2013.

[1] Balloon-borne stratospheric condensation nuclei (CN) measurements have been made from McMurdo Station, Antarctica (78°S), 1986–2010, and from Laramie, Wyoming (41°N), 1982 to the present. In the Antarctic region, the measurements show the formation of a layer of enhanced concentrations of stratospheric CN, between 21 and 27 km, around mid August, reaching its maximum extent between September and early October. CN concentrations increase from backgrounds of 10–20 cm^{-3} to over 100 cm^{-3} in the layer. In the northern midlatitudes, the measurements show a quasi-annual and smaller layer of enhanced CN concentrations between 25 and 31 km in late winter and early spring. In the quasi-annual layers, CN concentrations increase from backgrounds of 1–10 cm^{-3} to over 20 cm^{-3}. Volcanic eruptions appear to enhance the CN layers observed over Laramie and McMurdo. The Arctic Oscillation generally correlates with the magnitude of the Laramie CN layer, suggesting the importance of meridional transport. Volatility measurements and nucleation modeling support a sulfuric acid and water composition and binary homogeneous nucleation as the likely CN formation mechanism in both locations. Bimonthly measurements above Laramie support coagulation as the main reason for the dissipation of the CN layer. Air parcel trajectory modeling confirms that the CN layer forms locally to McMurdo and that it is related to solar exposure, while above Laramie trajectory analysis indicates that Arctic conditions and ambient temperature changes during northerly transport impact the magnitude of the CN layer above Laramie.

Citation: Campbell, P., and T. Deshler (2014), Condensation nuclei measurements in the midlatitude (1982–2012) and Antarctic (1986–2010) stratosphere between 20 and 35 km, *J. Geophys. Res. Atmos.*, *119*, doi:10.1002/2013JD019710.

1. Introduction

[2] Condensation nuclei (CN) are generally defined as nuclei mode particles (< 0.1 μm) upon which condensation begins in the atmosphere. In situ measurement of CN is accomplished by using CN counters, which cause aerosol to grow by condensation, thus allowing the smaller particles to reach optically detectable sizes. CN counters therefore not only measure the particles which were initially below optically detectable size but they also quantify the total number concentration of all aerosol above a specific critical size. The critical size is dependent on the working fluid and supersaturation of the instrument employed [*Miller and Bodhaine*, 1982; *McMurry*, 2000].

[3] Typical background stratospheric aerosol (SA) size distributions are dominated for number by particles ≈0.05 μm in radii [*Deshler et al.*, 2003]. Thus, all observations of the total concentration of SA, or likewise the CN concentration, arise from in situ measurements using CN counters. Satellites have a lack of sensitivity to particles with radii < 0.1 μm [*Thomason et al.*, 2008] and thus cannot be used to fully quantify CN concentrations. It is important to measure the CN concentration, however, as CN can serve as sites for condensation of additional gasses such as water vapor (H_2O) and sulfuric acid (H_2SO_4) in midlatitudes, while also nitric acid (HNO_3) in the polar regions. Considering that the numbers of CN are dominated by the smallest particles in the stratosphere, with negligible sedimentation rates, they may also be used as a tracer for transport processes.

[4] Following the landmark measurements by *Junge et al.* [1961], balloon-borne observations of stratospheric CN have continued since the 1970s in midlatitudes [*Rosen and Hofmann*, 1977; *Rosen et al.*, 1978; *Deshler et al.*, 2003] and 1980s in polar regions [*Hofmann and Rosen*, 1985; *Hofmann et al.*, 1989]. Stratospheric CN measurements have also been made from aircraft during the 1980s, 1990s, and 2000s [*Wilson et al.*, 1983, 1989, 1990, 1991; *Brock et al.*, 1995; *Borrmann et al.*, 2010].

[5] Balloon-borne stratospheric CN measurements by the University of Wyoming have been made on a consistent schedule (section 3) since the 1980s at Laramie, Wyoming (41°N), since 1986 at McMurdo Station, Antarctica (78°S), and at other sites ranging from the equatorial to the polar regions. This stratospheric CN record provides information on the general abundance of CN and some information on

[1]Department of Atmospheric Science, University of Wyoming, Laramie, Wyoming, USA.

Corresponding author: P. Campbell, University of Wyoming, Department of Atmospheric Science, 1000 East University Ave., Laramie, WY 82071, USA. (pcampbe2@uwyo.edu)

2169-897X/14/10.1002/2013JD019710

the sources of stratospheric CN. Mid-stratosphere (> 20 km) CN concentration enhancements during the late winter/early spring, referred to as "CN layers," have been observed in both midlatitude [*Rosen and Hofmann*, 1983] and polar regions [*Hofmann*, 1990b] and are a specific focus of this paper. The midlatitude CN layer has been suggested to originate in higher latitudes and to be intensified during volcanically active periods [*Hofmann et al*., 1985]. Theoretical investigations of the Antarctic CN layer have used microphysical models to probe its source [*Zhao et al*., 1995; *Mills et al*., 1999, 2005]. Until this time, however, a compilation of the stratospheric CN measurements at Laramie and McMurdo, in conjunction with their seasonality and the long-term record of CN layer events, has not been presented. Thus, the main goals of this paper are to present the 1982–2012 Laramie and 1986–2010 McMurdo CN measurements, with analyses of the annual and long-term patterns in CN concentrations, and to characterize CN layers in terms of their volatility and possible formation mechanisms in both locations.

2. Instrumentation and Uncertainties

2.1. CN Instrumentation

[6] In situ measurements of the total aerosol population typically require forcing particles to grow through condensation to optically detectable sizes. Various working fluids, ranging from water to butanol, and methods of supersaturation, from expansion to rapid cooling, have been used. The names Aitken and CN have been used interchangeably in the past, both implying large supersaturations for condensation, although generally, Aitken nuclei are reserved for particles sensed using water and expansion, in honor of the original measurements [*Aitken*, 1888]. Thus, Aitken nuclei counters are generally reserved for measurement using water as the working fluid, while CN counters imply other working fluids [*Podzimek and Carstens*, 1985]. Most commercial CN counters use butanol with various temperature gradients to achieve the desired supersaturation and thus detection size [e.g., *Wilson et al*., 1983; *Wiedensohlet et al*., 1997], while other working fluids have been used for specific applications [e.g., *Brock et al*., 2000].

[7] Balloon-borne measurements to 10 hPa or less require a less volatile working fluid. The measurements presented here use a 15 cm long heated cylinder coated with ethylene glycol that is evaporated into the sample air stream. The temperature of the walls in the saturator range from 25 to 35°C, increasing as pressure decreases. In the 15 cm long condenser, the wall temperature is decreased to 0°C to create a sudden supersaturation. The final design for this growth chamber was completed in the early 1980s [*Rosen and Hofmann*, 1981a, 1981b], leading to saturation ratios with respect to ethylene glycol ranging from 3.0 to 6.0 [*Rozier*, 1993]. For these growth chamber saturation ratios, the theoretical minimum observable particle size is ~0.001 μm radius. For balloon-borne measurements, this two-cylinder growth chamber is mounted vertically on top of an optical particle counter sensitive to particles > 0.15 μm radius [*Rosen*, 1964]. This instrument has been used to measure CN above Laramie since the early 1980s and above McMurdo since 1986. The concentration detection threshold for these CN instruments is ~0.01 cm^{-3}, one particle in a 10 s sampling interval.

2.2. Uncertainties

[8] The major uncertainties of these CN measurements are random uncertainty introduced by the reproducibility of a measurement and systematic uncertainties due to coincidence [*Sugita et al*., 1999], counting efficiency, and particle loss by diffusion. The random uncertainty is quantified by recent laboratory measurements which indicated an agreement of +/− 10%, with a standard deviation of 4%, between four identical but independent optical particle counters used for CN measurements. This agrees with previous laboratory measurements indicating precisions of +/− 10% for similar optical particle instruments [*Deshler et al*., 2003]. Of the systematic uncertainties, coincidence may be accounted for while pressure and size-dependent counting efficiency and particle loss by diffusion are more ambiguous.

[9] Coincidence is an issue at high CN concentrations and can be accounted for using [*van der Meulen et al*., 1980]

$$\frac{C}{C_o} = \exp(-C_o Q t_R) \tag{1}$$

where C is the observed number concentration, C_o the true number concentration, Q the instrument flow rate (≈13 $cm^3\ s^{-1}$), and t_R the electronics recovery time (≈ 60 μs). For the instruments used here, coincidence loss is 10% at observed (true) concentrations of 125 (140) cm^{-3}, increasing to 34% at observed (true) concentrations of 330 (500) cm^{-3}. This CN instrument saturates at observed (true) concentrations of about 450 (1000) cm^{-3}. Since particle concentrations are often 1000 cm^{-3} in the troposphere, a dilution system is used for midlatitude measurements until pressure decreases below 200 hPa. At lower pressures, higher altitudes, CN concentrations rarely exceed 50 cm^{-3}, except in polar regions, where stratospheric CN concentrations can be high in CN layers. Measured concentrations > 100 cm^{-3} are corrected for coincidence losses using equation 1.

[10] Laboratory measurements at pressures as low as 50 hPa indicated that the Wyoming CN counter has a counting efficiency exceeding 75% for particles as small as 0.003 μm radius, the minimum size which could be generated [*Rozier*, 1993]. These measurements allow us to define the lower size limit of the CN instrument < ≈0.003 μm radius, increasing to perhaps < ≈0.01 μm as pressures decrease below 50 hPa, although counting efficiency measurements at lower pressures have not been completed. Counting efficiencies at larger sizes and higher pressures varied but were also > 75%.

[11] Particle loss by diffusion of small particles to the inlet wall occurs prior to their entry to the condensation chamber. Due to the strong dependence of diffusional loss on size, $\propto r^{-2}$ for $r < 0.05$ μm, and the fact that the SA size distribution is not measured at the particle sizes which dominate the CN number, the magnitude of diffusional losses can only be bracketed. At 50 hPa, the diffusional loss for particles of 0.01–0.003 μm radius, with (without) the 20 cm long dilution valve, in addition to the 15 cm evaporation chamber, are about 15 (5)–55 (35) %, while at 10 hPa, the diffusional losses have a range of 35 (20)–95 (80) %. Thus, diffusional loss may be important above Laramie, as dilution valves are generally used here, and because the upper boundary of CN layers can be found at pressures near 10 hPa. Thus, it is possible that both CN concentrations near the top of CN layers, and the altitude of the upper boundary of the CN layer, may be underestimated.

[12] In summary, we conclude that there is a random uncertainty for the CN concentration measurements of +/− 10% with a systematic low bias of 25–50% dependent on particle size and pressure-dependent counting efficiency and diffusional loss, both of which cannot be explicitly accounted for because of a lack of size information in the SA at sizes which dominate the CN measurements. A systematic low bias of 25%, along with the random uncertainty of ±10%, is added to the error bars shown with the CN profile measurements but is not included in the analyses of the long-term CN concentration measurements.

2.3. Heated Inlet for Volatility Measurements

[13] The composition of SA (liquid droplets of H_2SO_4 and H_2O) has been tested with heated inlets [*Rosen*, 1971; *Deshler et al*., 1992] and more recently with mass spectrometric measurements [*Murphy et al*., 1998; *Arnold et al*., 1998]. The composition of newly formed particles in the upper troposphere and lower stratosphere has also been measured on several occasions with heated inlets [*Brock et al*., 1995; *Borrmann et al*., 2010]. *Brock et al*. [1995] found that there is a maximum in the binary homogeneous nucleation of H_2SO_4-H_2O particles within the upper tropical troposphere and that this source is a major factor controlling the number concentration of particles in the lower tropical and midlatitude stratosphere. *Borrmann et al*. [2010] further measured the geographical distribution of particle abundance in the upper tropical troposphere and lower stratosphere and in part confirmed that the upper tropical troposphere serves as a continuous source of particles for the maintenance of the global SA layer. *Borrmann et al*. [2010] also suggested that the source particles consist not only of H_2SO_4-H_2O but also of nonvolatile components.

[14] To extend these volatility measurements to the mid-stratosphere (> 20 km) CN layer, which forms over McMurdo, a heated inlet was developed to show whether the particles in the CN layer are predominantly volatile, thus indicative of a solution of H_2SO_4-H_2O or contain a nonvolatile core. The measurement required two CN instruments flown together, in which one of the instruments had a heated inlet prior to the particle growth system. The inlet was heated to 210°C and the length adjusted by the time necessary to reach temperature equilibrium inside the inlet [*Incropera and Dewitt*, 1990], plus the time necessary to evaporate a pure H_2SO_4-H_2O droplet from the particle growth/evaporation equation [*Pruppacher and Klett*, 1997]. Following particle evaporation, the inlet was cooled gradually by removing the heating element, to allow gasses to condense on the inlet walls. Heat transfer theory indicated that this inlet temperature was sufficient to volatilize H_2SO_4-H_2O droplets at air pressures below 50 hPa. While this inlet was not tested in the laboratory with H_2SO_4-H_2O droplets, other similar temperatures, some lower, have been used for higher pressures and have demonstrated complete vaporization of larger H_2SO_4-H_2O droplets [*Brock et al*., 1995; *Schmid et al*., 2002; *Borrmann et al*., 2010]. During a test flight out of Laramie in the spring of 2010, there was a weak CN layer observed. This observation stimulated further flights from Laramie following the McMurdo measurements.

3. Observations

[15] Measurements of CN are required to complete the SA size distribution measurements provided by companion in situ optical particle counters sensitive to aerosol between 0.15 and 10 μm radius and have been a primary use of such CN measurements [*Hofmann and Rosen*, 1982; *Deshler et al*., 2003]. These SA size distribution measurements from Laramie have documented both volcanic [*Hofmann and Rosen*, 1981, 1982; *Deshler et al*., 1992] and volcanically quiescent [*Hofmann*, 1990a; *Deshler et al*., 2003] aerosol. Those in the polar region have focused on polar stratospheric clouds [*Hofmann and Deshler*, 1991; *Deshler et al*., 1994] because of the role these clouds play in ozone loss [*Solomon et al*., 1986]. The measurements have also captured the development of enhanced particle concentrations, CN layers, which generally appear above 20 km over McMurdo and above 25 km over Laramie, and provided long-term measurements of the total number concentration of SA (> 0.003–0.01 μm) at altitudes and times away from the CN layers. These latter two points are the focus of the analysis presented here. CN observations have typically been made 6–12 times a year at Laramie and 2–3 times a year, between late August and early October, at McMurdo. The measurements at McMurdo have been extended to include earlier winter measurements during four of these years.

[16] Figure 1 presents CN concentration and temperature profiles seasonally averaged over Laramie (Figures 1a and 1b) and monthly averaged from June/July to October over McMurdo (Figures 1c and 1d). Figure 1, as well as all measurement profiles as a function of altitude in this paper, is presented in terms of geopotential height above mean sea level (ASL). This figure illustrates the relative stability of CN concentration with altitude over the measurement period at altitudes below 25 km at Laramie (Figure 1a) and with the exception of a few measurements in September and October that affect the average profile, below 20 km at McMurdo (Figure 1c). In the Laramie profiles (Figure 1a), there is a clear increase in CN concentration by a factor of 3–5 between 25 and 30 km in the winter and spring profiles, the CN layer. During this time, the temperature profiles (Figure 1b) vary minimally, typical of the midlatitude stratosphere. At McMurdo, the CN profiles (Figure 1c) capture the initiation, at times as early as June/July near 30 km, and the development of a CN layer between 20 and 25 km during austral winter-spring conditions, as demonstrated by the rapidly warming stratospheric temperatures (Figure 1d). The McMurdo CN layer increases in concentration and subsides into September, where concentrations have increased by factors of 5 to over 10, and then weakens in concentration into October. Characteristics of these profiles are typical of annual variations observed at Laramie, and of late winter-spring variations observed at McMurdo.

3.1. Seasonality

3.1.1. Laramie, Wyoming

[17] Figure 2 presents box-whisker plots of 2 km averages of balloon-borne CN concentration measurements, by month, over Laramie (21–35 km, 1982–2012). There is a clear quasi-annual variation in mid-stratosphere CN above Laramie. The average CN concentrations increase upon the start of winter, reach a maximum as spring begins, and then

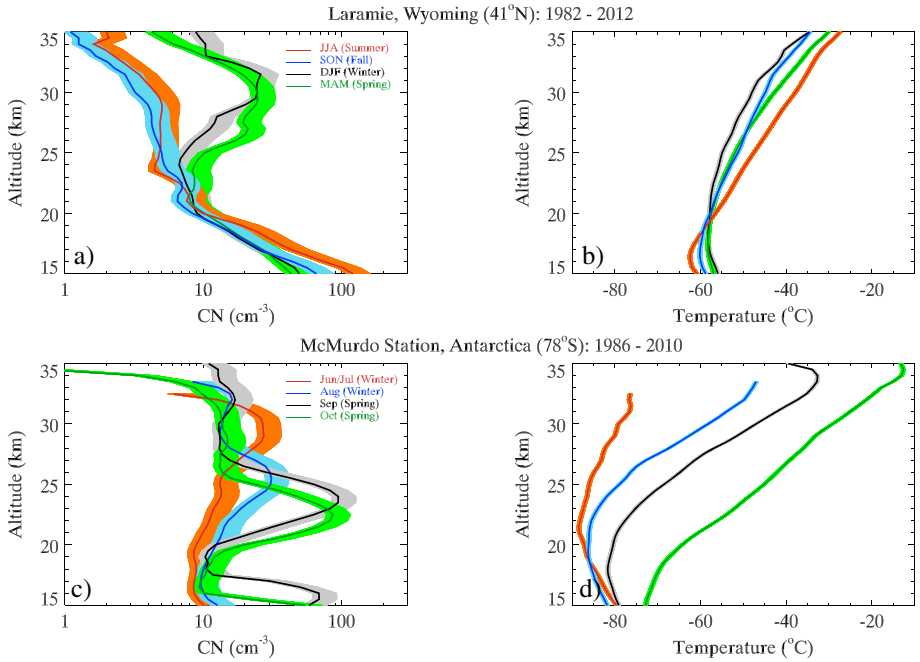

Figure 1. Averaged CN ($r > 0.003$–0.01 μm) and temperature profiles observed (a, b) above Laramie, Wyoming (41°N) for 1982–2012 and (c, d) above McMurdo Station, Antarctica (78°S) for 1986–2010. The data are seasonally averaged for Laramie and monthly averaged for McMurdo according to the legends in Figures 1a and 1c. The shaded areas indicate the −10 to + 35% uncertainty in the CN measurement, as discussed in the text, as well as a ± 0.5°C uncertainty for the temperature measurements.

decay into late summer/early fall. Further investigation of Figure 2 by altitude layers indicates that the major concentration enhancement occurs primarily between 25 and 31 km during winter and spring, with a maximum between 27 and 29 km in late winter. Below 25 km and above 33 km during the CN layer period (late winter to early spring), and at all altitudes (≈ 20–35 km) during the remainder of the year, the stratospheric CN concentrations have less of a quasi-annual cycle and are mainly within a range of about 1–10 cm^{-3} (Figures 1a and 2). Figure 2 also shows numerous outliers in the data, most prolific in winter and early spring. About 10 of these data points reached 2 km mean concentrations 100 cm^{-3} and may be defined as anomalously high CN layers. All of these CN layers were found at altitudes above 25 km. These anomalous CN layer events will be discussed further in the next section.

[18] Also in Figure 2 were three elevated CN layers, 2 km average CN concentrations > 20 cm^{-3}, which appeared between 21 and 23 km during summer (June and August) and fall (September), when CN layers are not usually observed above Laramie. Each of these three CN layers occurred within a few months of a major volcanic eruption and represented the distinct CN enhancements reported soon after volcanic eruptions [*Hofmann and Rosen*, 1981, 1982; *Deshler et al.*, 1992], which tend to disappear within approximately 3 months following the eruption [*Hofmann and Rosen*, 1982]. These layers are evidence of the fresh condensation of the sulfur gasses injected by these eruptions and are distinct from the higher altitude, and often higher concentration, CN layers which appear in winter/spring.

3.1.2. McMurdo Station, Antarctica

[19] Figure 3a presents a box-whisker analysis, similar to Figure 2, of the CN observations above McMurdo, which are only available in the winter and spring. Prior to polar sunrise above 18 km (≈ 8 August; Julian day 220) at McMurdo, the 2 km average CN concentrations are relatively constant with height; however, following sunrise, CN concentrations

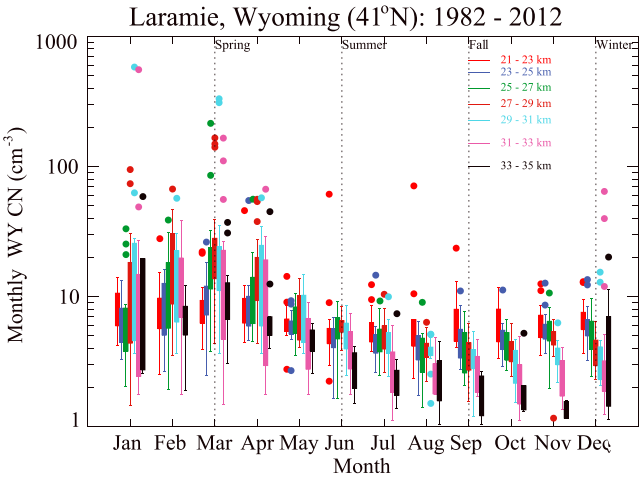

Figure 2. Box-whisker plots of the annual cycle, by month, of 2 km mean CN concentrations (color legend) between 21 and 35 km over Laramie since 1982. The data not included between the whiskers are plotted as an outlier with a small circle. The vertical dotted lines signify the start of each meteorological season for the Northern Hemisphere.

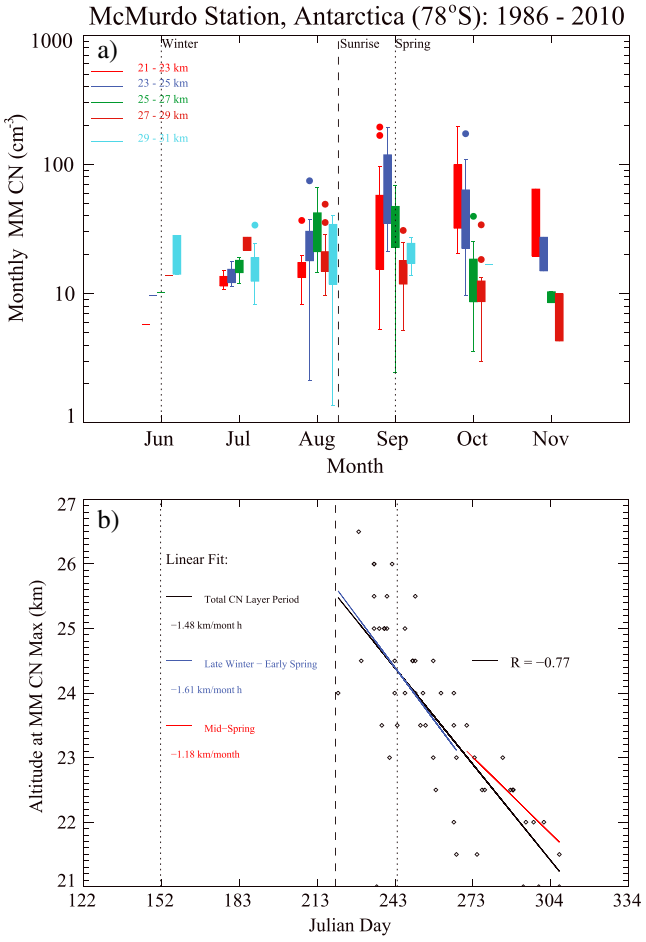

Figure 3. (a) Box-whisker plot of the winter/spring cycle, by month, of 2 km mean CN concentrations (color legend) between 21 and 31 km for McMurdo since 1986. The box-whisker plot is described similarly to Figure 2. (b) Altitude of CN layer maximum above McMurdo versus Julian day for McMurdo since 1986. The vertical dotted lines in Figures 3a and 3b signify the start of each meteorological season in the Southern Hemisphere, and the dashed vertical line in Figure 3b indicates the approximate day of polar sunrise above 18 km at McMurdo (Julian day = 220). The *R* value in Figure 3b indicates the Pearson correlation coefficient between altitude of CN maximum and Julian day.

increase in several altitude bands. The increase is greatest at 25–27 km in August, 23–25 km in September, and 21–23 km in October. Although these altitudes are lower than those of the springtime CN layers in Laramie, these altitudes cannot be compared directly due to differences in the structure of the stratosphere at the two locations. During this CN layer formation and growth period, CN concentrations begin to increase in August, peak in September, and then begin to decrease in October. The decrease is fastest at higher altitudes (25–27 km). By November, enhanced CN concentrations are found only at the lowest altitude range of 21–23 km. These observations are consistent with (1) initial nucleation of particles at high altitude, (2) particles subsiding to lower altitudes, and (3) termination of nucleation at higher altitudes, due to rapidly warming temperatures. This qualitative scenario is supported by the average CN and temperature profiles for McMurdo in Figures 1c and 1d. Below 21 km and above 27 km during the CN layer period (late winter to early spring), and at all altitudes (≈ 15–30 km) prior to the CN layer formation (early mid winter), the stratospheric CN concentrations are generally within 10–20 cm^{-3} (Figures 1b and 3a), with a few outliers.

[20] The anticorrelation of altitude of CN layer maximum and time, mentioned above, is presented in Figure 3b and has a correlation coefficient of −0.77. The slope of the altitude of layer maximum versus time in mid spring, when the CN layer is in its dissipation stage, proves to be a reasonable estimate of subsidence within the Southern Hemisphere polar vortex, suggesting this to be the reason for the decreasing altitude of the CN layer. *Manney et al.* [1994] estimated average vertical air velocities of ≈ −1.17 km/month at altitudes less than 23 km in the polar vortex over Antarctica. The subsidence of the observed CN layer in mid spring is calculated to be −1.18 km/month.

3.2. Stratospheric CN Record

[21] A history of the yearly maximum 2 km, and minimum 10 km, column average stratospheric CN concentrations between 21 and 31 km at McMurdo and 25 and 35 km at Laramie is shown in Figure 4. At Laramie, labels are included for the four highest (2 km average > 100 cm^{-3}) anomalous CN concentrations (A1–A4) from Figure 2, the CN maximum concentration in the year following the Mount Pinatubo eruption (P1), a relatively low CN maximum in the late 1990s (L1; 2 km average < 10 cm^{-3}), and the highest CN maximum in the two decades since the Pinatubo eruption (E1; 2 km average > 30 cm^{-3}). Although only a simple comparison, specific major volcanic eruptions that may have influenced the CN concentrations over Laramie, between 1982 and 2011, and McMurdo, between 1986 and 2010, are indicated by the vertical lines and labels (a–o) on the *x* axes of Figure 4. The volcanic eruptions included met the following criteria: a Volcanic Explosivity Index [*Newhall and Self*, 1982] ≥ 4, ensuring a definite stratospheric injection (cloud column height = 10–25 km), a Volcanic Sulfur Dioxide Index [*Schnetzler et al.*, 1997] ≥ 4, ensuring that the stratospheric injection included an abundant amount of SO_2 (SO_2 = 0.2–1 · 10^3 kt), and latitude between 90°S and 20°N for McMurdo and between 20°S and 90°N for Laramie. The volcanic eruption of Mount Ruiz, which had a Volcanic Explosivity Index of 3, was also included, given that it emitted a rich amount of SO_2 [*Krueger et al.*, 1990].

[22] At McMurdo, Figure 4a is suggestive of a period 1987–1995 with enhanced CN concentrations associated with an active volcanic period. Between 1995 and 2005, CN max concentrations are lower, although the data record is much thinner during this time. The gaps in the data represent years with no successful measurements or when measurements were only available after late October (Julian day ≈ 290) during the dissipation stages of the CN layer (Figure 3a). The low maximum in 1997 was measured in late September during the typical peak of the CN layer. An explanation for the weak CN layer in 1997 is not clear at this time. In the last 2 years of measurements, 2009 and 2010, the CN concentrations return to levels observed in the early 1990s. The lower CN maxima between 1996 and 2007 may be associated with the long period without eruptions, according to our criteria. The only two volcanic eruptions (k and l) which met the criteria for McMurdo after

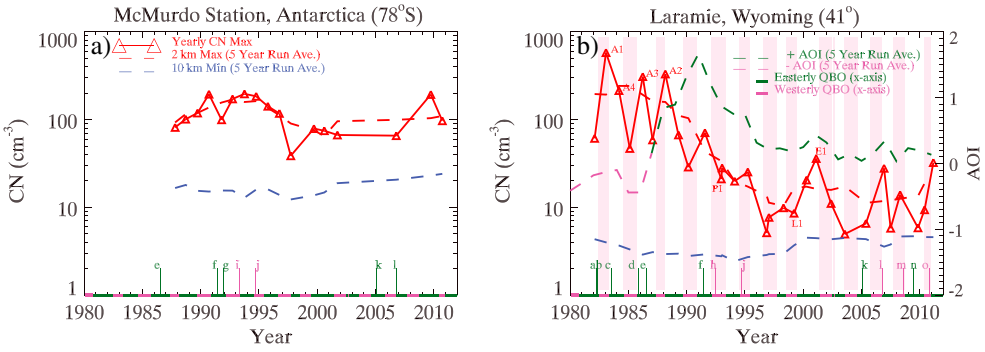

Figure 4. Annual 2 km CN concentration maximum, 5 year 2 km maximum running average, and 5 year 10 km minimum running average measured at (a) McMurdo and (b) Laramie, according to the legend in Figure 4a. In Figures 4a and 4b extended tick marks on the *x* axes represent volcanic eruptions (see criteria in text) and include the following: a; El Chichón, b; Galunggung, c; Colo, d; Ruiz, e; Nyamuragira, f; Pinatubo, g; Cerro Hudson, h; Spurr, i; Lascar, j; Rabaul (1994), k; Manam, l; Rabaul (2006), m; Kasatochi, n; Sarychev Peak, o; Merapi. Also in Figures 4a and 4b, the phase of the quasi-biennial oscillation (QBO) at 20 hPa has been coded on the *x* axes according to the legend in Figure 4b. The westerly QBO phase, after 1982, has been further shaded for comparison in Figure 4b. Also in Figure 4b, the 5 year running average of the winter season (January, February, and March) standardized mean Arctic Oscillation Index (AOI) has been included between 1980 and 2011. Also in Figure 4b, anomalous CN maxima (2 km average 100 cm^{-3}) are labeled A1–A4 (1983–1988), where P1 (1992) provides reference to a time period shortly following the Mount Pinatubo eruption. Finally, points L1 and E1 represent two other events, one relatively low (L1; 2 km average < 10 cm^{-3}) and high (E1; 2 km average > 30 cm^{-3}) CN layer maximum concentration, occurring in 1999 and 2001, respectively.

1995 occurred in 2005 and 2007. It has been suggested that volcanic activity has an effect on the CN layer maximum concentration above McMurdo [*Hofmann and Rosen*, 1985]. The CN record in Figure 4a is supportive of this claim.

[23] The minimum 10 km column CN concentration, i.e., background level, stays relatively constant through the changes described above, with the exception of a small increase following 2000. This confirms that with the exception of CN layer development at McMurdo, the mid-stratosphere (> 20 km) CN record has remained relatively undisturbed in late winter and spring, near the approximate background concentration of 10–20 cm^{-3} (Figure 4a).

[24] In contrast to McMurdo, the 2 km maximum CN concentrations at Laramie substantially decrease between 1982 and 1997, Figure 4b. The 5 year running average of the maximum concentrations between 1982 and 1990 remains above 100 cm^{-3} but begins to decrease after 1985. The yearly 2 km maximum fluctuates between 1982 and 1990, when the three largest anomalous peaks occur in 1983 (A1), 1988 (A2), and 1986 (A3) in conjunction with a volcanically active period (eruptions a-El Chichón, b-Galunggung, c-Colo, d-Ruiz, e-Nyamuragira). The anomalous CN layer in 1983, A1, has been attributed to the volcanic eruption of El Chichón (17°N, 93°W) on 4 April 1982. *Hofmann et al.* [1985] suggested that substantial warming in the polar region was sufficient to vaporize resident sulfuric acid aerosol derived mainly from the El Chichón eruption 10 months earlier and subsequently transported to the Arctic during winter. Following a stratospheric warming in the Arctic, the high-altitude air was transported to midlatitudes. Subsequent cooling and high H_2SO_4-H_2O supersaturations then led to enhanced nucleation of CN prior to observation at Laramie [*Hofmann et al.*, 1985]. Similar processes may explain other anomalous CN layer events over Laramie.

[25] Following 1988, there is a rather steady decrease in the yearly maximum concentration until 1997. During this time, the 10 km column CN minimum stays relatively constant, while increasing slightly following 2000, and agrees with McMurdo in that the midstratospheric CN concentrations are relatively static, with exception of the development of CN layers. At Laramie, the approximate background is about 1–10 cm^{-3} (Figure 4b). The slight increase in the background CN at both Laramie and McMurdo following 2000 may be associated with the increase in the background SA level over the past decade or so [*Hofmann et al.*, 2009], which has recently been attributed to increases in the number of relatively moderate volcanic eruptions [*Neely et al.*, 2013]. Between 1997 and 2005, there was no significant Northern Hemisphere volcanic activity, and the yearly maximum concentrations are lower by a factor of 10 compared to the 1980s, while the 5 year running average remains relatively constant. Following 2005, the fluctuating yearly maximum concentrations coincide with volcanic eruptions (k-Manam, l-Rabaul, m-Kasatochi, n-Sarychev Peak, o-Merapi) where two elevated maximum CN concentrations occur following eruptions (k, l and n, o). The other elevated yearly maximum in 2001 is not currently associated with any known eruption. It is worth noting that the data record has also thinned following the mid-1990s and the fluctuating CN layer maximum concentrations may be affected by timing of the infrequent observations.

[26] Although the peaks in maximum CN concentrations at Laramie almost all appear near volcanic eruptions, the eruptions of the early 1990s, the Mount Pinatubo eruption (f) and two lesser eruptions (h-Spurr and j-Rabaul), did not cause similar increases in the yearly maximum CN concentration as did eruptions in the surrounding periods. In fact, CN concentrations are largely decreasing during this period. Furthermore, the

Mount Pinatubo eruption (Volcanic Explosivity Index = 6) was much larger than any of the other eruptions and had arguably the largest stratospheric impact of the twentieth century [*McCormick et al*., 1995, Table 1]. Thus, an intriguing question remains. Why were the yearly maximum CN concentrations in the early 1990s, and those following the Mount Pinatubo eruption (P1), much smaller than the anomalous (A1–A4) yearly maximum concentrations during the 1980s? This question suggests that other processes in addition to volcanic eruptions affect the CN maxima at Laramie, such as atmospheric circulation and meridional transport.

[27] As suggested by *Hofmann et al*. [1985], enhanced CN concentrations over Laramie may result from meridional transport of volcanically perturbed aerosol to the Arctic followed by a return of high-altitude air from the Arctic to Laramie. Two modes of hemispheric variability, the quasi-biennial oscillation (QBO) and Arctic Oscillation (AO), play a role in these transport processes.

[28] The QBO, with a period of about 28 months [*Baldwin et al*., 2001], affects the stratospheric flow from pole to pole. The westerly phase of the QBO is associated with tropical deep convection, enhancement in vertical transport of aerosol into the stratosphere, and subsequent meridional transport poleward [*Choi et al*., 1998]. This phase of the QBO would be favorable for enhanced CN concentrations at Laramie, following volcanic eruptions. Figure 4b shows the phase of the QBO at 20 hPa, coded along the time axis and on each labeled volcanic eruption. During the yearly CN concentration maximums of the 1980s, which were large and highly variable, each of the labeled volcanic eruptions (a–e) occurred during an easterly QBO, three (c, d, e) at the beginning or middle, while (a, b) occurred right at the end of an easterly QBO. The maximum A1 then occurred in the following westerly QBO, but subsequent maxima occurred in both easterly and westerly phases of the QBO. The eruption of Mount Pinatubo (f) in 1991 occurred during an easterly QBO but was shortly followed by a transition into a westerly QBO, similar to A1 in 1983. The CN layer maximum P1 was, however, significantly less than A1. Figure 4b does not support a strong role of the QBO in the occurrence of CN layer maximums.

[29] The AO, characterized by the AO index (AOI), also affects the meridional transport from the Arctic to the midlatitudes [*Thompson and Wallace*, 1998]. A negative AOI is favorable for meridional transport of winter Arctic air to the midlatitudes with a positive AOI less favorable. In Figure 4b, there was an average negative AOI during the early to mid-1980s, thus allowing Arctic air to be more easily transported meridionally to Laramie. This was followed by a significant shift to a positive AOI in 1987 which peaked in 1991 and then decayed to remain slightly positive since 1997. With the shift to a positive AOI, the average maximum CN concentrations were significantly reduced. The eruption of Mount Pinatubo occurred during the strong positive phase of the AOI, and thus, its impact in enhancing CN concentrations above Laramie, similar to the volcanic eruptions in the 1980s [*Hofmann et al*., 1985], may have been significantly dampened. These ideas will be further explored in section 5.

4. Volatility of Stratospheric CN

[30] Figures 5a and 5b show results for the two volatility measurements at McMurdo during both the pre-CN layer (blue: 100829) and the post-CN layer formation (red: 100924) measurements. The nonvolatile fraction, f_{NV}, above and below the CN layer ($f_{NV}^{out} \approx 0.57$) is in good agreement between both measurements, indicating that over half the particles in the aged aerosol, although probably composed primarily of H_2SO_4 and H_2O, have a nonvolatile core larger than the detection threshold of the CN instrument ($r > 0.003$–0.01 μm, pressure dependent), which are perhaps of exoatmospheric origin. These f_{NV} values outside the CN layer are in agreement with those from *Curtius et al*. [2005], where they report a f_{NV} range of 0.58–0.76 for particles ($r > 0.01$ μm) in the Arctic lower stratosphere. The sharp decrease in f_{NV} within the CN layer ($f_{NV}^{in} < 0.10$) indicates predominantly pure H_2SO_4-H_2O solution droplets or at least droplets with nonvolatile cores smaller than the CN detection threshold, $r < 0.003$–0.01 μm. At the altitude of CN layer maximum and f_{NV} minimum on 100924 (≈ 22.5 km), subtracting the number of nonvolatile particles on 100829 from the number of nonvolatile particles within the CN layer on 100924, and then dividing by the total number of new particles, gives the nonvolatile fraction of only the newly nucleated particles within the CN layer, $f_{NV}^{new}, f_{NV}^{new} \approx 0.02$. Thus, within the CN layer, only approximately 2% of the particles contain a nonvolatile core. The observations in Figures 5a and 5b are consistent with models, which predict that the majority of the observable polar CN layer is due to binary homogeneous nucleation and condensation following rapid oxidation of SO_2 to H_2SO_4 [*Zhao et al*., 1995; *Mills et al*., 1999]. The observations have not been compared to models including ion-induced nucleation [*Lee et al*., 2003; *Lovejoy et al*., 2004]. These measurements disagree with the modeling of *Megner et al*. [2008], which suggests that nonvolatile meteoritic smoke particles with $r > 0.01$ μm comprise a *large* fraction of the enhanced particle concentrations observed in polar CN layers. Our results also qualify *Murphy et al*. [1998, 2013], where it is suggested that in polar winter, sulfuric acid primarily condenses on nonvolatile meteoritic material. Our results are in general agreement with this, except in the CN layers with significant, and rapid, formation of new particles without a nonvolatile core.

[31] CN profiles measured above Laramie in 2012 (120322–120920), including two with volatility measurements (120322 in red, 120920 in blue), are shown in Figures 5c and 5d. In addition, a third volatility measurement on 100601 (in black) is included. A weak CN layer was captured in 2010, while a strong CN layer was observed on 120322 and on all subsequent CN profiles in 2012, capturing the decay of the 2012 layer. The magnitude of the Laramie CN layer on 120322 ($> 30\ cm^{-3}$) is enhanced compared to the overall record during the past 20 years (Figure 4b).

[32] Average stratospheric flow in 2012 was investigated using the National Centers for Environmental Prediction (NCEP) reanalysis data (see http://www.esrl.noaa.gov/psd/data/gridded/data.ncep.reanalysis.pressure.html). The monthly average stratospheric flow at 10 hPa was predominantly zonal over North America during 2012, with the exception of late February through mid-March, which exhibited strong northerly flow from the high to midlatitudes (not shown). The enhanced Laramie CN layer on 120322 was measured subsequent to this northerly flow, thus supportive of an impact from Arctic transport. The sharp lower boundary of the CN layer near 25–26 km on 120322 is suggestive of recent formation, as an aged layer

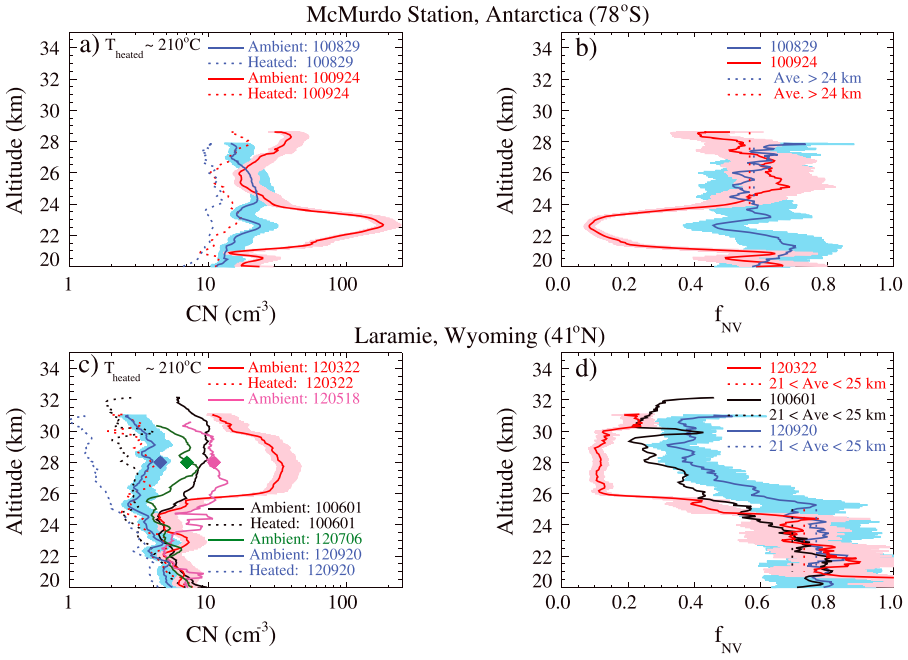

Figure 5. Ambient (solid lines) and heated (dotted lines) CN profiles at (a) McMurdo on 100829 (blue) and 100924 (red) and (c) Laramie on 120322 (red), 100601 (black), and 120920 (blue). The approximate temperature of the heated instruments is also listed in Figures 5a and 5c. Fraction of nonvolatile particles from the CN layer volatility measurements at (b) McMurdo and (d) Laramie. Green and purple solid lines in Figure 5c are ambient CN profiles, measured between the two volatility measurements in 2012. Vertical dotted lines in Figures 5b and 5d represent the vertical average of nonvolatile particle fractions above 24 km at McMurdo and between 21 and 25 km at Laramie. Filled diamonds in Figure 5c represent simple coagulation calculations at 28 km over the time periods (~ 2 months) between measurements of ambient CN profiles. The light red and blue shading in Figures 5a and 5c represents the measurement uncertainty (−10 to + 35%) for two ambient profiles at McMurdo and Laramie, while the shading in Figures 5b and 5d represents the approximate uncertainty (+/− 20%) for the fraction of nonvolatile particles.

would be expected to have a broader boundary due to mixing to lower altitudes, which is observable on subsequent profiles. The final volatility measurement in fall 2012 (120920) is near the minimum in seasonal mid-stratosphere, midlatitude, CN concentrations (see Figure 2).

[33] The single CN profile measured in June 2010 is consistent with the dissipation of the CN layer observed in 2012, as the June 2010 (100601) profile falls between the profiles measured in May (120518) and July (120706) 2012. This suggests that there may have been a similar Laramie CN layer in 2010 but unobserved due to a lack of measurements in early 2010. The previous CN measurement was in November 2009.

[34] Between 21 and 25 km, below the CN layer, Figure 5d indicates good agreement for the 120322, 100601, and 120920 average f_{NV}. This corroborates previous findings, which suggest that at these altitudes, the majority of the aerosol contains some meteoritic dust [*Hunten et al.*, 1980; *Turco et al.*, 1981; *Hervig et al.*, 2009]. In fact, between 20 and 24 km, there is good agreement between our average f_{NV} ($f_{NV}^{out} \approx 0.74$) and the 60–70% reported in *Neely et al.* [2011, Figure 1].

[35] Above 25 km, within the 120322 CN layer at Laramie, f_{NV}^{in} is similar to measurements from McMurdo, Figure 5b, decreasing to < 0.10 when the layer is substantially enhanced on 120322. This indicates that similar to McMurdo, the CN layer above Laramie is also primarily composed of binary H_2SO_4-H_2O solution droplets. To explain the formation of this layer using classical binary homogeneous nucleation models [e.g., *Jaecker-Voirol and Mirabel*, 1988; *Noppel*, 1998] would require transport from a colder region. Midlatitude stratospheric temperatures (Figure 1b) are too warm generally, and specifically for 120322, to predict new particle formation in the midlatitude stratosphere above 20 km. Other nucleation possibilities, such as ion induced, would also be similarly dependent on temperature and unlikely to reproduce the observations for local nucleation. Considering the northerly flow preceding the measurement on 120322, the need for colder temperatures for any particle nucleation process, and the sharp lower boundary, the layer on 120322 is suggestive of recent high-latitude particle formation from gaseous H_2O-H_2SO_4 and subsequent transport to the midlatitudes. During the 100601 and 120920 measurements, the f_{NV} in the region of the previous CN layer increases to about 0.3 and 0.4, respectively, indicating that a larger fraction of the ambient CN is mixed with nonvolatile cores as the layer decays, although this fraction is still less than in the air beneath the CN layer.

[36] On 100601, there is a peculiar sharp peak in the f_{NV} near 30 km, where the data in Figure 5d, which are smoothed, indicate a f_{NV} equal to about 0.43. Notice the narrow layer at 30 km in the heated profile on 100601. For the nonsmoothed data (not shown), the f_{NV} is even larger in this thin layer, equal to about 0.75, and is less than at 1 km thick. This peak in f_{NV} was measured on both balloon ascent and descent.

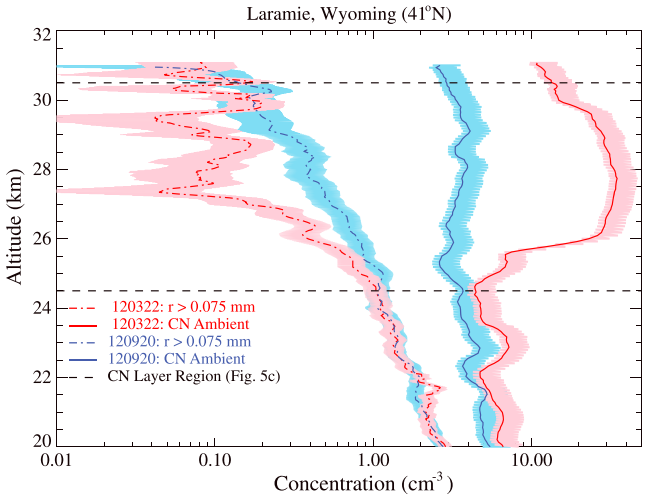

Figure 6. Coincident ambient CN (solid lines) and larger ($r > 0.075$ μm) aerosol (dashed-dotted lines), measured on 120322 (red) and 120920 (blue) at Laramie. The horizontal dashed lines represent the region of the CN layer measured on 120322 (see Figure 5c). The uncertainty (light red and blue) for the CN concentrations is the same as in Figure 5c. The larger aerosol uncertainty (light red and blue) is dominated by Poisson counting statistics at these low concentrations.

There is no current explanation for this narrow nonvolatile layer at the top of the CN layer.

[37] Comparison of the ambient CN profiles on 120322, 120518, 120706, and 120920, about every 2 months, demonstrates a clear dissipation of the CN layer, a transition from a sharp to diffuse lower boundary, and an increase in the nonvolatile fraction. This decay of a midlatitude CN layer represents specifically the measurements summarized earlier (Figure 2). The concentration of the nonvolatile CN also decreases between 120322 and 120920, at altitudes above 25 km, even as the nonvolatile fraction increases. This decay in concentration in the CN layer is probably due to coagulation. To test this idea, Figure 6 shows measurements of larger aerosol, $r > 0.075$ μm, which were also measured on 120322 and 120920. Within the altitude band of the CN layer, coinciding with the decrease in ambient CN, there was an increase in the concentration of particles with $r > 0.075$ μm between 120322 and 120920. This increase in concentration of larger particles was not apparent below the CN layer and is suggestive of an increasing number of larger particles due to coagulation within the high concentrations of the CN layer.

[38] A simple polydisperse coagulation calculation at 28 km was carried out using a coagulation coefficient, K, of $122 \cdot 10^{-16}$ m^{-3} s^{-1} [*Hinds*, 1999, Table 12.3], which is representative of coagulation between particles of 0.05 and 0.005 μm in radius. The radius of 0.05 μm is just smaller than the larger aerosol size ($r > 0.075$) shown in Figure 6, in which there was an increase in concentration. This calculation allows for both the coagulation of particles of similar size and for a few larger CN ($r \approx 0.05$ μm) to scavenge the smaller volatile particles ($r \approx 0.005$ μm) nucleated in the CN layer. Beginning with the initial CN concentration at 28 km on 120322, CN concentrations due to coagulation were calculated for each subsequent CN measurement, approximately every 2 months following 120322, and are shown as diamonds in Figure 5c, color coded to match the respective profiles. Although a simple approximation, the results are in good agreement with the observed ambient CN layer at 28 km. The decrease in the nonvolatile CN concentrations within the CN layer, from 120322 to 120920, Figure 5c, indicates that in the CN layer where coagulation is most rapidly occurring, the nonvolatile CN were also coagulating. Their concentration decreased by about half. Overall, as the CN coagulate and grow, they increase the larger particle concentration and, as coagulation occurs amongst some of the nonvolatile particles, along with the volatile ones, both the nonvolatile and volatile CN concentrations are reduced, with the volatile being reduced faster due to their larger concentrations and smaller sizes leading to coagulation with any available particle.

5. CN Layer Formation

[39] To investigate the formation of the mid-stratosphere CN layer over McMurdo and Laramie, we consider here nucleation modeling, solar exposure, and air parcel trajectory analysis.

5.1. Nucleation Modeling

[40] To compare with stratospheric CN observations, a classical binary homogeneous nucleation (CBHN) model was developed for the nucleation of H_2SO_4-H_2O solution droplets. Although CBHN theory includes uncertainty from its capillarity approximation [*Laaksonen and Napari*, 2001; *Kalikmanov*, 2010] and has differences in magnitude when compared to empirically measured CBHN rates [*Wyslouzil et al.*, 1991], studies have indicated that classical theory qualitatively agrees with atmospheric regions of enhanced particle formation [*Brock et al.*, 1995], especially in the stratosphere [*Mills et al.*, 1999]. Thus, CBHN models are effective at predicting where a mid-stratosphere CN layer should occur. As described in *Jaecker-Voirol and Mirabel* [1988], a hydrated version of the CBHN rate, J, is given by

$$J = X_h C_h \exp\left(-\frac{\Delta G^*}{kT}\right) \quad (2)$$

where X_h is the hydrate-corrected frequency factor, C_h the hydrate correction factor, ΔG^* the change in Gibbs free energy

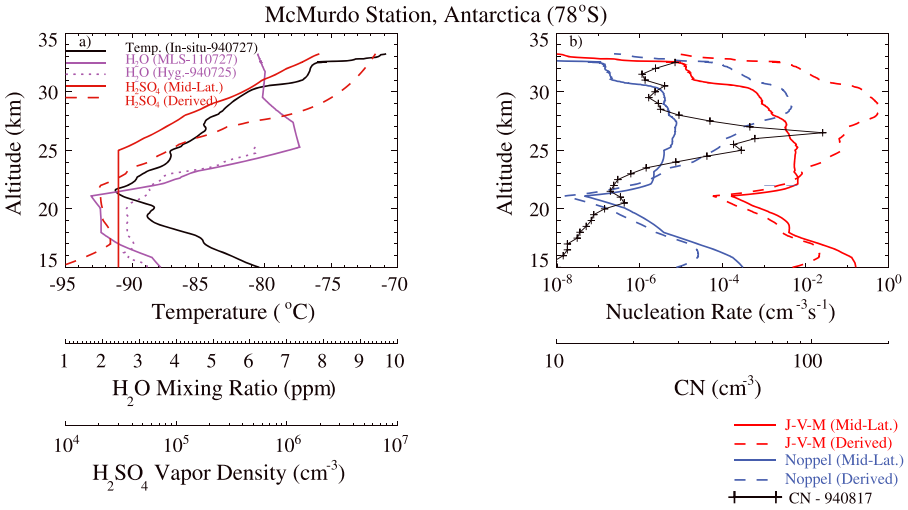

Figure 7. (a) Ambient temperature (black solid), H_2O mixing ratio (purple solid), and midlatitude (brown solid) and derived polar H_2SO_4 vapor density (brown dashed) profiles used for the models. A balloon-borne hygrometer H_2O mixing ratio measurement (purple dotted) is also shown for comparison in Figure 7a. (b) CBHN model runs based on two hydrated model formulations (red: J-V-M; blue: Noppel), compared to the CN observation ($r > 0.003$–0.01 μm) at McMurdo on 940817 (plus symbols). In Figure 7b, the solid and dashed lines represent the CBHN calculations using the midlatitude and derived polar H_2SO_4 vapor density profiles, respectively.

of the critical cluster (i.e., height of the nucleation barrier), k the Boltzmann's constant, and T the ambient temperature. In this form of J, the hydrate correction to the kinetic term comes from X_h, whereas the correction to the energetic term ΔG^* comes from C_h. Thus, ΔG^* refers to $\Delta G^*_{\text{unhyd}}$, the uncorrected free energy. For more details regarding CBHN and hydrate theory, the reader is referred to *Heist and Reiss* [1974], *Jaecker-Voirol et al.* [1987], *Jaecker-Voirol and Mirabel* [1988, 1989], *Noppel* [1998, 2000], *Noppel et al.* [2002], and *Seinfeld and Pandis* [2006, Chapter 11].

[41] The following describes a comparison between observations and CBHN model calculations, based on hydrated CBHN formulations of *Jaecker-Voirol and Mirabel* [1988], i.e., J-V-M (equation 2), and *Noppel* [1998], i.e., Noppel, for McMurdo during the late winter of 1994. The full model details are not described here; however, the details on calculating the critical variables can be found in the following sources: surface tension [*Vehkamaki et al.*, 2002], density [*Luo et al.*, 1996], H_2SO_4 equilibrium vapor pressure [*Kulmala and Laaksonen*, 1990], and H_2O equilibrium vapor pressure [*Tabazadeh et al.*, 1997]. The calculation of a profile of CBHN rates requires profiles of temperature and H_2O and H_2SO_4 vapor density (Figure 7a). The CBHN calculations here used in situ balloon-borne temperature measurements on 940727, and an H_2O vapor-mixing ratio profile, measured on 110727 by the Microwave Limb Sounder (MLS) on the Aura satellite [*Waters et al.*, 2006]. The MLS H_2O vapor-mixing ratio measurement was preferred over a unique balloon-borne hygrometer measurement on 940725 [*Vömel et al.*, 1995] (Figure 7a), as this hygrometer sounding had a ceiling of only 25.5 km. The comparison between the MLS and hygrometer measurements, however, is in good agreement below 25.5 km. This agreement provides confidence for the use of the 110727 MLS measurement in the CBHN calculations (Figure 7a). To complete model calculations requires a H_2SO_4 vapor density profile, but none is available over the southern polar regions; however, midlatitude stratospheric H_2SO_4 measurements have been made in the past [*Arnold and Fabian*, 1980; *Arnold et al.*, 1981; *Viggiano and Arnold*, 1981, 1983; *Arnold and Buhrke*, 1983; *Schlager and Arnold*, 1987; *Reiner and Arnold*, 1997]. Here an approximate H_2SO_4 vapor density profile is used, which is based on a compilation of midlatitude stratospheric H_2SO_4 measurements [*Mills et al.*, 2005, Figure 1]. The H_2SO_4 vapor density profile here is assumed constant at $3{\cdot}10^5$ cm^{-3} up to 25 km, followed by an increase to $2{\cdot}10^6$ cm^{-3} above 30 km (Figure 7a).

[42] The CBHN rates (J-V-M and Noppel), as well as the McMurdo CN observations about 3 weeks later on 940817, are shown in Figure 7b. The differences in magnitude between the two hydrated CBHN theories are due to the different hydrate correction methods discussed in *Jaecker-Voirol and Mirabel* [1988] and *Noppel* [1998]. Both CBHN models predict an enhancement in the formation of new particles in a layer between 20 and 30 km. There is an increase in the CBHN rates from about 21 to 27 km, and a sharp decrease in rates above 30 km. The overall region of enhanced nucleation rates in late July are in decent agreement with the observation of an initial CN layer at these altitudes on 940817, although there are distinct differences. Considering that an average midlatitude H_2SO_4 vapor density profile was used for a polar region, these differences are not surprising. As a check on how different a polar H_2SO_4 profile could be, the observed McMurdo CN concentration, temperature, and H_2O vapor density, along with CBHN theory, were used to derive an approximate H_2SO_4 vapor density profile, more representative of austral spring, where currently there are no measurements.

[43] The method approximates an "in situ nucleation rate," J, from the average difference in CN concentrations between all presunrise and 2 week post sunrise (> 18 km) McMurdo CN measurements (1986–2010). The average in situ nucleation rate and the averaged presunrise and post sunrise temperature

measurements were then used with a H_2O measurement near polar sunrise above McMurdo (100817), from MLS, to invert the CBHN equations and solve for an approximate polar H_2SO_4 vapor density profile, shown in Figure 7a. Although a single H_2O MLS profile was used, it remains representative of the average conditions above McMurdo in August, as is further confirmed by comparison, at similar times of the year, with water vapor profiles from in situ measurements at McMurdo in 1994 [*Vömel et al*., 1995].

[44] Overall, there is some confidence in the structure of the derived polar H_2SO_4 profile, although its magnitude is subject to uncertainty considering the difference between observable CN concentrations ($r > 0.003$–0.01 μm), used to infer the nucleation rate and smaller unobservable particles. Thus, the inferred nucleation rate is likely an underestimate of the true nucleation rate, leading to a subsequent underestimation in the magnitude of the derived H_2SO_4 profile. Above 25 km, the derived polar H_2SO_4 profile has a steeper slope and is larger by a factor of 6 on average, compared to the midlatitude profile. For completeness, the derived H_2SO_4 profile was then used to calculate new nucleation rates which are shown in Figure 7b and not surprisingly are in better agreement with observations. The qualitative agreement between the CBHN models and observations supports binary homogeneous nucleation as the primary formation mechanism for the mid-stratosphere polar CN layer. In the absence of measurements, this method of deriving a polar H_2SO_4 vapor density profile may be used to better represent H_2SO_4 conditions typical of south polar austral spring.

[45] This analysis has not considered preexisting aerosol and the surface area they present for supersaturated vapor, which would reduce the supersaturation and thus the nucleation rate. Estimates of preexisting aerosol surface area can be obtained from measurements of CN and aerosol with radius > 0.1 μm using a second optical particle counter. Such measurements are available and have been fit with unimodal/bimodal lognormal size distributions and the aerosol surface area calculated following *Deshler et al*. [2003]. For the McMurdo measurements, the aerosol surface in the region of the CN layer in late August was 2–4 $\mu m^2\,cm^{-3}$. This is significantly larger than the surface areas observed in the CN layer above Laramie on 120322. In this case the preexisting aerosol surface area can be estimated by imposing a CN profile typical for background CN on the larger aerosol measurements and comparing the surface area with and without a CN layer. For 120322, this results in surface areas of 0.1–0.2 $\mu m^2\,cm^{-3}$, increasing by about a factor of 3 when the CN layer is included. These surface areas are larger than any reasonable concentration (100–1000 cm^{-3}) of particles below 3 nm, so the existence of a large population of particles below the detection limit of the CN counter used would not significantly change these surface areas. Thus, the CN layers have formed within a wide range of preexisting aerosol surface areas, yet these were not sufficient to prevent new particle formation.

5.2. Solar Exposure

[46] Since polar winter temperatures near 25 km are $< -80°$ C, the relatively constant nucleation rate will be controlled by the H_2SO_4 vapor. The atmospheric formation of H_2SO_4 vapor is a result of the oxidation of SO_2, through reaction with the hydroxyl radical (OH) [*Calvert and Stockwell*, 1983; *Stockwell and Calvert*, 1983], which is dependent on the return of sunlight to the polar region during late winter [*Zhao et al*., 1995; *Mills*, 1996; *Mills et al*., 1999]. To test this idea, the solar flux ($W\,m^{-2}$) from the Hybrid Single-Particle Lagrangian Integrated Trajectory (HYSPLIT) model [*Draxler and Rolph*, 2013] was used to compare an air parcel's solar exposure, during a 2 week trajectory around Antarctica, with the CN layers observed as the air parcel arrived above McMurdo. Solar exposure is defined as the total solar flux an air parcel experiences over a period of time. It was calculated by integrating the solar flux over each 2 week back trajectory (315 h), ending at the time and altitude of each CN layer observation at McMurdo.

[47] Figure 8 shows a comparison between the column averaged (21–27 km) CN concentrations for all (1986–2010) McMurdo measurements between August and mid-September and their associated trajectories' column averaged (21–27 km) solar exposure. These months were chosen because they correspond to the time period of returning sunlight and CN layer formation above McMurdo (Figure 3a). Also included in Figure 8 are the mean and standard deviation of ensemble HYSPLIT trajectories for three points, low, middle, and high column CN concentrations, to give a sense of the uncertainty associated with a single HYSPLIT trajectory. Results from Figure 8 indicate that as the air parcel's solar exposure increases, the magnitude of the CN concentration between 21 and 27 km also increases. The correlation coefficient is 0.81. This highlights the importance of solar exposure and thus the presence of the OH radical and the subsequent oxidation of SO_2 into H_2SO_4. As the amount of H_2SO_4 increases, so do the CBHN rates and magnitude of the mid-stratosphere polar CN layer.

5.3. Transport to Midlatitudes

[48] As was previously discussed, enhanced CN layers observed over Laramie may be influenced by a warm Arctic vortex, increased evaporation of resident H_2SO_4-H_2O aerosol, amplified transport of this air to midlatitudes, and fresh nucleation of H_2SO_4-H_2O aerosol during the transport [*Hofmann et al*., 1985]. To further investigate this effect on the development of CN layers, HYSPLIT air parcel trajectories were analyzed for selected CN layers observed above Laramie. For this analysis, the ambient temperature along a HYSPLIT trajectory was used to calculate the H_2SO_4 saturation ratio [*Hamill et al*., 1977] as

$$S = \frac{P_S}{P_S^o(r)}^{\chi} \frac{P_W}{P_W^o(r)}^{1-\chi} \tag{3}$$

where P is the partial pressure of sulfuric acid and water, $P^o(r)$ the Kelvin-corrected equilibrium partial pressure for sulfuric acid and water, and χ the molecular fraction of sulfuric acid molecules, within the last 5 days of the 2 week back trajectory ending at an altitude of 30 km ASL at Laramie. The ending time periods chosen for the HYSPLIT trajectories were coincident with the yearly maximum CN concentrations labeled in Figure 4b (A1–A4; E4; P1; L1). The calculation of S used a constant H_2O mixing ratio of 5 ppm, since the effect of H_2SO_4-H_2O condensation on the concentration of water vapor is negligible, and allowed the H_2SO_4 mixing ratio to change as temperature along the trajectory changed. Temperature affects S through the $P^o(r)$

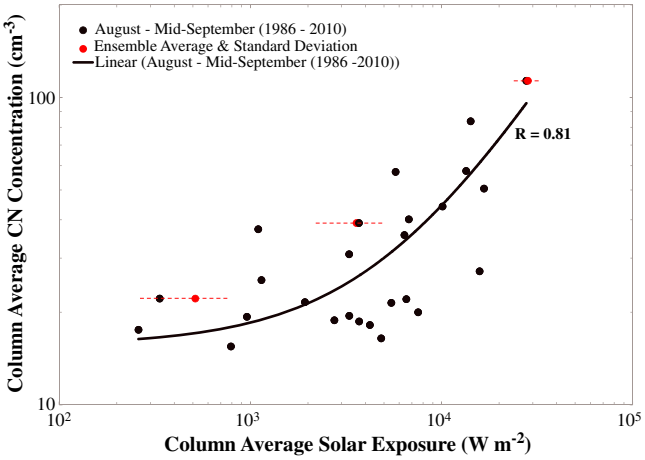

Figure 8. Column averaged (21–27 km) CN concentrations above McMurdo observed during August–September between 1986 and 2010, versus the column averaged (21–27 km) solar exposure calculated from the integrated solar flux along the HYSPLIT 2 week (315 h) back trajectory for each CN measurement. Included for three points (in red), low, middle, and high column CN concentrations, are their average and standard deviations for ensemble HYSPLIT solar exposures.

and χ terms and in turn alters the H_2SO_4 mixing ratio. Each trajectory was initialized assuming an H_2SO_4 mixing ratio that would give an $S = 1$ at the start of the trajectory. As temperature changes, condensation ($S > 1$) or nucleation ($S > 3$) may occur and deplete the H_2SO_4 vapor, or evaporation ($S < 1$) may occur and increase the H_2SO_4 vapor.

[49] The results for the 5 day back trajectories associated with the anomalously high CN layers A1–A4 and E1 in Figure 4b are shown in Figure 9, compared with two events with no significant enhancement in CN concentration, P1 and L1 also in Figure 4b. Also included are the mean and standard deviation of the ensemble HYSPLIT trajectories for A1. Each back trajectory is labeled with a latitude indicating its highest northern excursion. In all cases with significant CN layers (A1–A4, E1), the air parcels experienced increasing temperatures leading to H_2SO_4 evaporation and

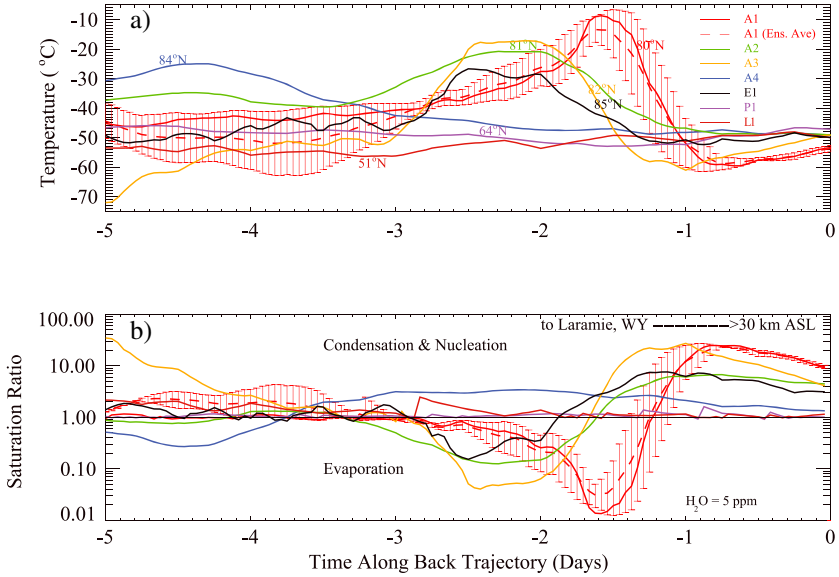

Figure 9. (a) Temperature along 2 week HYSPLIT back trajectories, for only the last 5 days prior to arrival above Laramie (30 km ASL), ending at the time of CN observations. The end points of the trajectories pertain to the four anomalously high CN concentration measurements, A1–A4, the smaller maximum CN measurement following the Mount Pinatubo eruption, P1, a relatively low maximum CN concentration during 1999, L1, and the elevated CN concentration during 2001, E1 (see Figure 4b). The maximum latitudinal excursion of each trajectory is labeled at the time of occurrence along the back trajectory. (b) Calculated H_2SO_4 saturation ratio over stratospheric aerosol along the back trajectory. The horizontal black line at $S = 1$ represents the separation between possible evaporation and condensation/nucleation. Also included for trajectory A1 are the average and standard deviation for the ensemble HYSPLIT temperature and saturation ratio, dashed red lines.

then cooling prior to arrival at Laramie. For the highest anomalous case, A1, as discussed in *Hofmann et al*. [1985], the extent of warming and subsequent cooling in the high-latitude region along the trajectory is the greatest. For A1, at about 1.5 days prior to reaching Laramie, the air temperature at 72°N reached −9°C and then cooled rapidly, at about 5° C h^{-1}, as the air parcel approached Laramie. This results in a sharp change in the saturation ratio regime from evaporation to nucleation. For the other most significant Laramie CN layers A2, A3, A4, and E1, the maximum temperatures are −21, −17, −25, and −27°C, respectively, the trajectories oscillate in temperature and saturation ratios, suggestive of warming and evaporation followed by cooling and nucleation, and the oscillations in temperature and saturation histories are similar to A1 but with weaker amplitudes. The A4 trajectory indicates rather low cooling rates and thus maximum saturation ratios near the nucleation threshold of three. The general correlation between A1–A3 and E1's amplitudes of oscillation in Figure 9, and magnitude of associated CN layers in Figure 4b, suggests that enhanced CN layers observed above Laramie may be influenced by polar stratospheric warming/evaporation and subsequent cooling/nucleation as the air parcels reach the midlatitudes. It is also clear from Figure 9a that A1–A4 and E1 all have maximum latitudinal positions of > 80°N, indicating that these 5 day parcel trajectories had traversed through extreme high latitudes, possibly within the polar vortex although the air parcels were not confined to the vortex. This suggests a strong chance of stratospheric warming and vortex splitting during these back trajectories, which is consistent with the maximum temperatures occurring near the point of highest latitude excursion as suggested by *Hofmann et al*. [1985].

[50] In contrast to the anomalous and elevated CN layer events, the smaller CN enhancements of P1 and L1 are characterized by temperature and saturation ratio histories showing little variation. In fact, although P1 and L1 are representatives of a similar early springtime period as A1–A4 and E1, the temperature along their back trajectories remains relatively steady and saturation ratios remain near 1. Furthermore, the P1 and L1 air parcel trajectories have lower maximum latitudinal positions of < 65°N, indicating that the 5 day trajectory was predominantly outside the polar vortex, and there was no opportunity to pass through a region of stratospheric warming as evidenced by their static temperatures near −50°C.

[51] Results from Figure 9 suggest that transport from high latitudes is associated with the formation of elevated CN layers in the Laramie record if the air along that transport also experiences other factors such as (1) polar stratospheric warming and evaporation of preexisting aerosol, (2) subsequent cooling and thus increase in saturation ratio; and (3) fresh nucleation of particles during transport. The magnitude of these latter three factors appears to be important influences on the magnitude of the observed CN layers above Laramie.

6. Discussion

[52] The CN measurements presented here are based on periodic in situ balloon-borne profile measurements, which are made in an Eulerian reference frame, from Laramie, Wyoming, and McMurdo Station, Antarctica. The periodicity of the measurements has changed over the years ranging from 3 to 12 per year at Laramie and 0 to 3 at McMurdo for August–October. Thus, between the measurements, there are large-scale horizontal circulations transporting stratospheric air both zonally and meridionally. In spite of these variations, clear seasonal cycles are observed for the Laramie CN concentrations between 20 and 30 km, Figure 2, over the past 30 years. More recently, for observations over 6 months, during the Laramie volatility measurements in 2012, Figure 5c, the dissipation of CN concentrations appeared to be satisfactorily described considering only coagulation processes expected within an air parcel. With the exception of late February to mid-March 2012, which was representative of strong northerly flow and enhanced CN layer concentrations (Figure 5c; 120322), the monthly averaged NCEP reanalysis data indicated generally zonal flow at 10 hPa through 2012. This flow pattern coupled with the observations suggests a globally extensive CN layer traveling in the large-scale zonal stratospheric circulation, such that the 2012 periodic observations at a single site were able to capture changes controlled primarily by local processes occurring within the air mass. Since similar local processes would be occurring throughout a global CN layer, periodic temporal sampling may be sufficient to capture the evolution of CN concentrations. In fact, there are no other good options since only in situ measurements are capable of measuring CN.

[53] Past observations by balloon [e.g., *Rosen et al*., 1975; *Deshler et al*., 2003], lidar [*Jäger*, 2005], aircraft [e.g., *McCormick and Swissler*, 1983; *Reeves et al*., 2008], and satellite [e.g., *Thomason et al*., 1997, 2008] instruments indicate that SA have a global extent, during both volcanically active and quiescent periods [*Deshler et al*., 2006]. The Laramie CN observations and our simple models of the evolution of CN concentration suggest that the stratospheric CN layer is global as well, at least as far as Laramie, with enhancements in the CN concentration coinciding with northerly transport. This suggests a global CN layer dependent upon the time of year, transport in the stratosphere, vortex conditions, and perturbations by volcanic eruptions. Testing the idea that long-term observations of stratospheric CN at two point locations, Laramie and McMurdo, can be used for a more global understanding requires work on this topic utilizing large-scale modeling (e.g., Community Earth System Model) to compare with the observations and to extend them.

7. Conclusions

[54] Measurements of stratospheric CN concentrations, monthly to bimonthly, from 1982 to 2012 over Laramie, Wyoming, in the northern midlatitudes, and seasonally August–October from 1986–2010 over McMurdo Station, Antarctica, in the high southern latitudes, were presented and analyzed. Seasonal analysis indicated a frequent late winter to early spring mid-stratosphere CN layer above Laramie and a late winter CN layer above McMurdo. The measurements show that the layers are observed between 25 and 31 km at Laramie and between 21 and 27 km at McMurdo. The McMurdo CN layer reaches its maximum concentration about 50 days after polar sunrise (late September) and then decreases as temperatures increase and end any further CN nucleation. On average, the McMurdo CN layer subsides during midspring at a rate of 1.2 km $month^{-1}$, which is consistent with subsidence of air in the polar vortex.

Investigation of the Laramie CN record showed a large decrease in the maximum CN concentrations since the 1980s. The records also indicate that volcanic eruptions impact the magnitude of the CN enhancements at both Laramie and McMurdo. In addition, the correlation between Laramie CN layers and the AOI suggested that enhanced midlatitude CN layers may be connected with high-altitude transport of air from northern latitudes and that a positive AOI may result in a dampening in the magnitude of maximum CN concentration in the face of volcanic eruptions. The seasonal and long-term records indicate that mid-stratospheric CN concentrations are relatively constant with altitude if CN layers are excluded and remain near background concentrations of 1–10 and 10–20 cm^{-3} at Laramie and McMurdo, respectively.

[55] The observed Laramie and McMurdo CN layers are both predominantly composed of H_2SO_4-H_2O solution droplets based on volatility measurements in both locations. The formation of these layers is consistent with classical binary homogeneous nucleation modeling. Models including ion-induced nucleation were not tested, and thus, the role of ions cannot be determined here. The evolution of CN concentrations within CN layers deduced from periodic, bimonthly measurements, was consistent with coagulation expected for particles traveling in a relatively undisturbed air parcel. These conclusions hold for both midlatitude and polar CN layers and suggest that the CN layers could have a global extent depending on the time of year. This is a topic of further investigation with global climate models.

[56] Air parcel trajectory analyses confirmed that an air parcel's solar exposure, while circulating around the Antarctic continent during late winter into early spring, is correlated with the magnitude of the CN layer observed at McMurdo. Trajectory analyses also provided evidence to suggest that the magnitude of CN layers at midlatitudes, such as those observed at Laramie during the 1980s, may be influenced by stratospheric warming in the high northern latitudes, evaporation of preexisting aerosol, and CN nucleation as the air parcel cools and is transported to the observation point of Laramie.

[57] **Acknowledgments.** These measurements over the years have required the work of many individuals; notable among these are Jim Rosen, Dave Hofmann, Bryan Johnson, Stephen Woods, Bruno Nardi, Jennifer Mercer, and a large number of technicians and engineers both in Laramie and at McMurdo. Similarly, the measurements have required funding from several agencies under a number of grants but primarily from the National Science Foundation (NSF). Current measurements are supported by the NSF under grant ATM-1011827. The recent McMurdo measurements were supported by the NSF under grant OPP-0839124.

References

Aitken, J. (1888), On the number of dust particles in the atmosphere, *Trans. R. Soc. Edinburgh*, *35*(1), 1–19.

Arnold, F., and T. Buhrke (1983), New H_2SO_4 and HSO_3 vapour measurements in the stratosphere—Evidence for a volcanic influence, *Nature*, *301*, 293–295, doi:10.1038/301293a0.

Arnold, F., and R. Fabian (1980), First measurements of gas phase sulphuric acid in the stratosphere, *Nature*, *283*, 55–57, doi:10.1038/283055a0.

Arnold, F., R. Fabian, and W. Joos (1981), Measurements of the height variation of sulfuric acid vapor concentrations in the stratosphere, *Geophys. Res. Lett.*, *8*, 293–296, doi:10.1029/GL008i003p00293.

Arnold, F., J. Curtius, S. Spreng, and T. Deshler (1998), Stratospheric aerosol sulfuric acid: First direct in situ measurements using a novel balloon-based mass spectrometer apparatus, *J. Atmos. Chem.*, *30*(1), 3–10, doi:10.1023/A:1006067511568.

Baldwin, M. P., et al. (2001), The quasi-biennial oscillation, *Rev. Geophys.*, *39*, 179–229, doi:10.1029/1999RG000073.

Borrmann, S., et al. (2010), Aerosols in the tropical and subtropical UT/LS: In-situ measurements of submicron particle abundance and volatility, *Atmos. Chem. Phys.*, *10*, 5573–5592, doi:10.5194/acp-10-5573-2010.

Brock, C. A., P. Hamill, J. C. Wilson, H. H. Jonsson, and K. R. Chan (1995), Particle formation in the upper tropical troposphere: A source of nuclei for the stratospheric aerosol, *Science*, *270*, 1650–1653, doi:10.1126/science.270.5242.1650.

Brock, C. A., F. Schröder, B. Kärcher, A. Petzold, R. Busen, and M. Fiebig (2000), Ultrafine particle size distributions measured in aircraft exhaust plumes, *J. Geophys. Res.*, *105*(D21), 26,555–26,567, doi:10.1029/2000JD900360.

Calvert, J. G., and W. R. Stockwell (1983), The mechanism and rates of the gas phase oxidations of sulfur dioxide and nitrogen oxides in the atmosphere, in *Acid Precipitation: SO_2, NO and NO_2 Oxidation Mechanisms: Atmospheric Considerations*, chap. 1, edited by J. G. Calvert, pp. 1–61, Ann Arbor Science Publishers, Ann Arbor, MI.

Choi, W., W. B. Grant, J. H. Park, K.-M. Lee, H. Lee, and J. M. Russell III (1998), Role of the quasi-biennial oscillation in the transport of aerosols from the tropical stratospheric reservoir to midlatitudes, *J. Geophys. Res.*, *103*(D6), 6033–6042, doi:10.1029/97JD03118.

Curtius, J., et al. (2005), Observations of meteoric material and implications for aerosol nucleation in the winter Arctic lower stratosphere derived from in situ particle measurements, *Atmos. Chem. Phys.*, *5*, 3053–3069, doi:10.5194/acp-5-3053-2005.

Deshler, T., D. J. Hofmann, B. J. Johnson, and W. R. Rozier (1992), Balloonborne measurements of the Pinatubo aerosol size distribution and volatility at Laramie, Wyoming during the summer of 1991, *Geophys. Res. Lett.*, *19*, 199–202, doi:10.1029/93GL01337.

Deshler, T., B. J. Johnson, and W. R. Rozier (1994), Changes in the character of polar stratospheric clouds over Antarctica in 1992 due to the Pinatubo volcanic aerosol, *Geophys. Res. Lett.*, *21*, 273–276, doi:10.1029/94GL00072.

Deshler, T., M. E. Hervig, D. J. Hofmann, J. M. Rosen, and J. B. Liley (2003), Thirty years of in situ stratospheric aerosol size distribution measurements from Laramie, Wyoming (41°N), using balloon-borne instruments, *J. Geophys. Res.*, *108*(D5), 4167, doi:10.1029/2002JD002514.

Deshler, T., R. Anderson-Sprecher, H. Jäger, J. Barnes, D. J. Hofmann, B. Clemesha, D. Simonich, M. Osborn, R. G. Grainger, and S. Godin-Beekmann (2006), Trends in the nonvolcanic component of stratospheric aerosol over the period 1971–2004, *J. Geophys. Res.*, *111*, D01201, doi:10.1029/2005JD006089.

Draxler, R. R., and G. D. Rolph (2013), HYSPLIT model access via NOAA ARL Real-time Environmental Applications and Display System (READY) Website, http://ready.arl.noaa.gov/HYSPLIT.php, NOAA ARL, Silver Spring, MD.

Hamill, P., C. S. Kiang, and R. D. Cadle (1977), The nucleation of H_2SO_4-H_2O solution aerosol particles in the stratosphere, *J. Atmos. Sci.*, *34*, 150–162, doi:10.1175/1520-0469(1977)034.

Heist, R. H., and H. Reiss (1974), Hydrates in supersaturated binary sulfuric acid-water vapor, *J. Chem. Phys.*, *61*, 573–581, doi:10.1063/1.1681932.

Hervig, M. E., L. L. Gordley, L. E. Deaver, D. E. Siskind, M. H. Stevens, J. M. Russell III, S. M. Bailey, L. Megner, and C. G. Bardeen (2009), First satellite observations of meteoric smoke in the middle atmosphere, *Geophys. Res. Lett.*, *36*, L18805, doi:10.1029/2009GL039737.

Hinds, W. C. (1999), *Aerosol Technology: Properties, Behavior, and Measurement of Airborne Particles*, pp. 323–331, Wiley-Interscience, Hoboken, NJ.

Hofmann, D. J. (1990a), Increase in the stratospheric background sulfuric acid aerosol mass in the past 10 years, *Science*, *248*, 996–1000, doi:10.1126/science.248.4958.996.

Hofmann, D. J. (1990b), Measurement of the condensation nuclei profile to 31 km in the Arctic in January 1989 and comparisons with Antarctic measurements, *Geophys. Res. Lett.*, *17*, 357–360, doi:10.1029/GL017i004p00357.

Hofmann, D. J., and T. Deshler (1991), Stratospheric cloud observations during formation of the Antarctic ozone hole in 1989, *J. Geophys. Res.*, *96*, 2897–2912, doi:10.1029/90JD02494.

Hofmann, D. J., and J. M. Rosen (1981), Stratospheric aerosol and condensation nuclei enhancements following the eruption of Alaid in April 1981, *Geophys. Res. Lett.*, *8*, 1231–1234, doi:10.1029/GL008i012p01231.

Hofmann, D. J., and J. M. Rosen (1982), Balloon-borne observations of stratospheric aerosol and condensation nuclei during the year following the Mt. St. Helens eruption, *J. Geophys. Res.*, *87*, 11,039–11,061, doi:10.1029/JC087iC13p11039.

Hofmann, D. J., and J. M. Rosen (1985), Antarctic observations of stratospheric aerosol and high altitude condensation nuclei following the El Chichón eruption, *Geophys. Res. Lett.*, *12*, 13–16, doi:10.1029/GL012i001p00013.

Hofmann, D. J., J. M. Rosen, and W. Gringel (1985), Delayed production of sulfuric acid condensation nuclei in the polar stratosphere from El Chichón volcanic vapors, *J. Geophys. Res.*, *90*, 2341–2354, doi:10.1029/JD090iD01p02341.

Hofmann, D. J., J. M. Rosen, J. W. Harder, and J. V. Hereford (1989), Balloon-borne measurements of aerosol, condensation nuclei, and cloud particles in the stratosphere at McMurdo Station, Antarctica, during the spring of 1987, *J. Geophys. Res.*, *94*, 11,253–11,269, doi:10.1029/JD094iD09p11253.

Hofmann, D., J. Barnes, M. O'Neill, M. Trudeau, and R. Neely (2009), Increase in background stratospheric aerosol observed with lidar at Mauna Loa Observatory and Boulder, Colorado, *Geophys. Res. Lett.*, *36*, L15808, doi:10.1029/2009GL039008.

Hunten, D. M., R. P. Turco, and O. B. Toon (1980), Smoke and dust particles of meteoric origin in the mesosphere and stratosphere, *J. Atmos. Sci.*, *37*, 1,342–1,357, doi:10.1175/1520-0469(1980)037.

Incropera, F. P., and D. P. Dewitt (1990), *Fundamentals of Heat and Mass Transfer*, John Wiley, Hoboken, NJ.

Jaecker-Voirol, A., and P. Mirabel (1988), Nucleation rate in a binary mixture of sulfuric acid and water vapor, *J. Phys. Chem.*, *92*, 3518–3521, doi:10.1021/j100323a039.

Jaecker-Voirol, A., and P. Mirabel (1989), Heteromolecular nucleation in the sulfuric acid-water system, *Atmos. Environ.*, *23*, 2053–2057, doi:10.1016/0004-6981(89)90530-1.

Jaecker-Voirol, A., P. Mirabel, and H. Reiss (1987), Hydrates in supersaturated binary sulfuric acid–water vapor: A reexamination, *J. Phys. Chem.*, *87*, 4849–4852, doi:10.1063/1.452847.

Jäger, H. (2005), Long-term record of lidar observations of the stratospheric aerosol layer at Garmisch-Partenkirchen, *J. Geophys. Res.*, *110*, D08106, doi:10.1029/2004JD005506.

Junge, C. E., C. W. Chagnon, and J. E. Manson (1961), Stratospheric aerosols, *J. Meteorol.*, *18*, 81–108, doi:10.1175/1520-0469.

Kalikmanov, V. I. (2010), Binary nucleation beyond capillarity approximation, *Phys. Rev.*, *81*, 050,601, doi:10.1103/PhysRevE.81.050601.

Krueger, A. J., L. S. Walter, C. C. Schetzler, and S. D. Doiron (1990), TOMS measurement of the sulfur dioxide emitted during the 1985 Nevado del Ruiz eruptions, *J. Volcanol. Geotherm. Res.*, *41*, 7–15, doi:10.1016/0377-0273(90)90081-P.

Kulmala, M., and A. Laaksonen (1990), Binary nucleation of water–sulfuric acid system: Comparison of classical theories with different H_2SO_4 saturation vapor pressures, *J. Chem. Phys.*, *93*, 696–701, doi:10.1063/1.459519.

Laaksonen, A., and I. Napari (2001), Breakdown of the capillarity approximation in binary nucleation: A density functional study, *J. Phys. Chem.*, *105*, 11,678–11,682, doi:10.1021/jp0116454.

Lee, S. H., J. M. Reeves, J. C. Wilson, D. E. Hunton, A. A. Viggiano, T. M. Miller, J. O. Ballenthin, and L. R. Lait (2003), Particle formation by ion nucleation in the upper troposphere and lower stratosphere, *Science*, *301*, 1886–1889, doi:10.1126/science.1087236.

Lovejoy, E. R., J. Curtius, and K. D. Froyd (2004), Atmospheric ion-induced nucleation of sulfuric acid and water, *J. Geophys. Res.*, *109*, D08204, doi:10.1029/2003JD004460.

Luo, B. P., U. K. Krieger, and T. Peter (1996), Densities and refractive indices of $H_2SO_4/HNO_3/H_2O$ solutions to stratospheric temperatures, *Geophys. Res. Lett.*, *23*, 3707–3710, doi:10.1029/96GL03581.

Manney, G. L., R. W. Zurek, A. O'Neill, and R. Swinbank (1994), On the motion of air through the stratospheric polar vortex, *J. Atmos. Sci.*, *51*, 2973–2994, doi:10.1175/1520-0469(1994)051.

McCormick, M. P., and T. J. Swissler (1983), Stratospheric aerosol mass and latitudinal distribution of the El Chichón eruption cloud for October 1982, *Geophys. Res. Lett.*, *10*, 877–880, doi:10.1029/GL010i009p00877.

McCormick, M. P., L. W. Thomason, and C. R. Trepte (1995), Atmospheric effects of the Mt. Pinatubo eruption, *Nature*, *373*, 399–404, doi:10.1038/373399a0.

McMurry, P. H. (2000), The history of condensation nuclei counters, *Aerosol Sci. Technol.*, *33*, 297–322, doi:10.1080/02786820050121512.

Megner, L., D. E. Siskind, M. Rapp, and J. Gumbel (2008), Global and temporal distribution of meteoric smoke: A two-dimensional simulation study, *J. Geophys. Res.*, *113*, D03202, doi:10.1029/2007JD009054.

van der Meulen, A., A. Plomp, F. Oeseburg, E. Buringh, R. M. van Aalst, and W. Hoevers (1980), Intercomparison of optical particle counters under conditions of normal operation, *Atmos. Environ.*, *14*, 495–499, doi:10.1016/0004-6981(80)90215-2.

Miller, S. W., and B. A. Bodhaine (1982), Supersaturation and expansion ratios in condensation nuclei counters: An historical perspective, *J. Aerosol Sci.*, *13*(6), 481–490, doi:10.1016/0021-8502(82)90014-3.

Mills, M. J. (1996), Stratospheric sulfate aerosol: A microphysical model, Ph.D. thesis, Univ. of Colo., Boulder.

Mills, M. J., O. B. Toon, and S. Solomon (1999), A 2D microphysical model of the polar stratospheric CN layer, *Geophys. Res. Lett.*, *26*(8), 1133–1136, doi:10.1029/1999GL900187.

Mills, M. J., O. B. Toon, V. Vaida, P. E. Hintze, H. G. Kjaergaard, D. P. Schofield, and T. W. Robinson (2005), Photolysis of sulfuric acid vapor by visible light as a source of the polar stratospheric CN layer, *J. Geophys. Res.*, *110*, D08201, doi:10.1029/2004JD005519.

Murphy, D. M., D. S. Thomson, and M. J. Mahoney (1998), In situ measurements of organics, meteoritic material, mercury, and other elements in aerosols at 5 to 19 kilometers, *Science*, *282*, 1664–1669, doi:10.1126/science.282.5394.1664.

Murphy, D. M., K. D. Froyd, J. P. Schwarz, and J. C. Wilson (2013), Observations of the chemical composition of stratospheric aerosol particles, *Q. J. R. Meteorol. Soc.*, doi:10.1002/qj.2213.

Neely III, R. R., J. M. English, O. B. Toon, S. Solomon, M. Mills, and J. P. Thayer (2011), Implications of extinction due to meteoritic smoke in the upper stratosphere, *Geophys. Res. Lett.*, *38*, L24808, doi:10.1029/2011GL049865.

Neely, R. R., III, et al. (2013), Recent anthropogenic increases in SO_2 from Asia have minimal impact on stratospheric aerosol, *Geophys. Res. Lett.*, *40*, 999–1004, doi:10.1002/grl.50263.

Newhall, C. G., and S. Self (1982), The volcanic explosivity index (VEI): An estimate of explosive magnitude for historical volcanism, *J. Geophys. Res.*, *87*, 1231–1238, doi:10.1029/JC087iC02p01231.

Noppel, M. (1998), Binary nucleation of water–sulfuric acid system: A reexamination of the classical hydrates interaction model, *J. Chem. Phys.*, *109*, 9052–9056, doi:10.1063/1.477575.

Noppel, M. (2000), Enthalpy and entropy changes in formation of gas phase sulfuric acid monohydrates and dehydrates as a result of fitting to experimental pressure data, *J. Geophys. Res.*, *105*, 19,779–19,785, doi:10.1029/2000JD900192.

Noppel, M., H. Vehkamäki, and M. Kulmala (2002), An improved model for hydrate formation in sulfuric acid–water nucleation, *J. Chem. Phys.*, *116*, 218–228, doi:10.1063/1.1423333.

Podzimek, J., and J. C. Carstens (1985), The 100 year evolution of Aitken nuclei counters: Current and future problems, *J. Rech. Atmos.*, *19*, 257–274.

Pruppacher, H., and J. Klett (1997), *Microphysics of Clouds and Precipitation*, Kluwer Academic Publisher, Norwell, MA.

Reeves, J. M., J. C. Wilson, C. A. Brock, and T. P. Bui (2008), Comparison of aerosol extinction coefficients, surface area density, and volume density from SAGE II and in situ aircraft measurements, *J. Geophys. Res.*, *113*, DI1202, doi:10.1029/2007JD009357.

Reiner, T., and F. Arnold (1997), Stratospheric SO_3: Upper limits inferred from ion composition measurement: Implications for H_2SO_4 and aerosol formation, *Geophys. Res. Lett.*, *24*, 1751–1754, doi:10.1029/97GL01758.

Rosen, J. M. (1964), Vertical distribution of dust to 30 kilometers, *J. Geophys. Res.*, *69*, 4673–4676, doi:10.1029/JZ069i021p04673.

Rosen, J. M. (1971), The boiling point of stratospheric aerosols, *J. Appl. Meteorol.*, *10*, 1044–1046, doi:10.1175/1520-0450(1971)010.

Rosen, J. M., and D. J. Hofmann (1977), Balloonborne measurements of condensation nuclei, *J. Appl. Meteorol.*, *10*, 56–62, doi:10.1175/1520-0450(1977)016.

Rosen, J. M., and D. J. Hofmann (1981a), Stratospheric condensation nuclei (Report No. AP – 61), Department of Physics and Astronomy, University of Wyoming, Laramie, Wyoming.

Rosen, J. M., and D. J. Hofmann (1981b), Stratospheric condensation nuclei (Report No. AP – 68), Department of Physics and Astronomy, University of Wyoming, Laramie, Wyoming.

Rosen, J. M., and D. J. Hofmann (1983), Unusual behavior in the condensation nuclei concentration at 30 km, *J. Geophys. Res.*, *88*, 3275–3731, doi:10.1029/JC088iC06p03725.

Rosen, J. M., D. J. Hofmann, and J. Laby (1975), Stratospheric aerosol measurements II: The worldwide distribution, *J. Atmos. Sci.*, *32*, 1457–1462, doi:10.1175/1520-0469(1975)032.

Rosen, J. M., D. J. Hofmann, and K. H. Kaselau (1978), Vertical profiles of condensation nuclei, *J. Appl. Meteorol.*, *17*, 1737–1740, doi:10.1175/1520-0450(1978)017.

Rozier, W. R. (1993), Analysis of a balloonborne, continuous flow condensation nuclei growth chamber, M.S. thesis, 85 pp., University of Wyoming, Laramie, Wyoming.

Schlager, H., and F. Arnold (1987), Balloon-borne composition measurements of stratospheric negative ions and inferred sulfuric acid vapor abundances during the Map/Globus 1983 campaign, *Planet. Space Sci.*, *35*, 693–701, doi:10.1016/0032-0633(87)90136-X.

Schmid, O., B. Eimer, D. E. Hagen, and P. D. Whitefield (2002), Investigation of volatility method for measuring aqueous sulfuric acid on mixed aerosols, *Aerosol Sci. Technol.*, *36*, 877–889, doi:10.1080/02786820290038519.

Schnetzler, C. C., G. J. S. Bluth, A. J. Krueger, and L. S. Walter (1997), A proposed volcanic sulfur dioxide index (VSI), *J. Geophys. Res.*, *102*, 20,087–20,091, doi:10.1029/97JB01142.

Seinfeld, J. H., and S. N. Pandis (2006), *Atmospheric Chemistry and Physics. From Air Pollution to Climate Change*, 2nd ed., John Wiley, Hoboken, NJ.

Solomon, S., R. R. Garcia, F. S. Rowland, and D. J. Wuebbles (1986), On the depletion of Antarctic ozone, *Nature*, *321*, 755–758, doi:10.1038/321755a0.

Stockwell, W. R., and J. G. Calvert (1983), The mechanism of the HO-SO_2 reaction, *Atmos. Environ.*, *17*, 2231–2235, doi:10.1016/0004-6981(83)90220-2.

Sugita, T., Y. Kondo, M. Koike, M. Kanada, N. Toriyama, H. Nakajima, T. Deshler, and R. Imasu (1999), Balloon-borne optical counter for in situ aerosol measurements, *J. Atmos. Chem.*, *32*, 183–204, doi:10.1023/A:1006128527288.

Tabazadeh, A., O. B. Toon, S. L. Clegg, and P. Hamill (1997), A new parameterization of H_2SO_4/H_2O aerosol composition: Atmospheric implications, *Geophys. Res. Lett.*, *24*, 1931–1934, doi:10.1029/97GL01879.

Thomason, L. W., L. R. Poole, and T. Deshler (1997), A global climatology of stratospheric aerosol surface area density deduced from Stratospheric Aerosol and Gas Experiment II measurements: 1984–1994, *J. Geophys. Res.*, *102*, 8967–8976, doi:10.1029/96JD02962.

Thomason, L. W., S. P. Burton, B. P. Luo, and T. Peter (2008), SAGE II measurements of stratospheric aerosol properties at non-volcanic levels, *Atmos. Chem. Phys.*, *8*, 983–995, doi:10.5194/acp-8-983-2008.

Thompson, D. W., and J. M. Wallace (1998), The Arctic Oscillation signature in the wintertime geopotential height and temperature fields, *Geophys. Res. Lett.*, *25*, 1297–1300, doi:10.1029/98GL00950.

Turco, R. P., O. B. Toon, P. Hamill, and R. C. Whitten (1981), Effects of meteoric debris on stratospheric aerosols and gases, *J. Geophys. Res.*, *86*, 1113–1128, doi:10.1029/JC086iC02p01113.

Vehkamaki, H., M. Kulmala, I. Napari, K. E. J. Lehtinen, C. Timmreck, M. Noppel, and A. Laaksonen (2002), An improved parameterization for sulfuric acid–water nucleation rates for tropospheric and stratospheric conditions, *J. Geophys. Res.*, *107*(D22), doi:10.1029/2002JD002184.

Viggiano, A. A., and F. Arnold (1981), Extended sulfuric acid vapor concentration measurements in the stratosphere, *Geophys. Res. Lett.*, *8*, 583–586, doi:10.1029/GL008i006p00583.

Viggiano, A. A., and F. Arnold (1983), Stratospheric sulfuric acid vapor: New and updated measurements, *J. Geophys. Res.*, *88*, 1457–1462, doi:10.1029/JC088iC02p01457.

Vömel, H., S. J. Oltmans, D. J. Hofmann, T. Deshler, and J. M. Rosen (1995), The evolution of the dehydration in the Antarctic stratospheric vortex, *J. Geophys. Res.*, *100*, 13,919–13,926, doi:10.1029/95JD01000.

Waters, J. W., et al. (2006), The Earth Observing System Microwave Limb Sounder (EOS MLS) on the Aura Satellite, *IEEE Trans. Geosci. Remote Sens.*, *44*, 1075–1092, doi:10.1109/TGRS.2006.873771.

Wiedensohlet, A. D., et al. (1997), Intercomparison study of the size-dependent counting efficiency of 26 condensation particle counters, *Aerosol Sci. Tech.*, *27*, 224–242, doi:10.1080/02786829708965469.

Wilson, J. C., J. H. Hyun, and E. D. Blackshear (1983), The function and response of an improved stratospheric condensation nucleus counter, *J. Geophys. Res.*, *88*, 6781–6785, doi:10.1029/JC088iC11p06781.

Wilson, J. C., M. Lowenstein, D. W. Fahey, B. Gary, S. D. Smity, K. K. Kelly, G. V. Ferry, and K. R. Chan (1989), Observations of condensation nuclei in the Airborne Antarctic Ozone Experiment: Implications for new particle formation and polar stratospheric cloud formation, *J. Geophys. Res.*, *94*, 16,437–16,448, doi:10.1029/JD094iD14p16437.

Wilson, J. C., M. R. Stolzenburg, W. E. Clark, M. Loewenstein, G. V. Ferry, and K. R. Chan (1990), Measurements of condensation nuclei in the Airborne Arctic Stratospheric Expedition: Observations of particle production in the polar vortex, *Geophys. Res. Lett.*, *17*, 361–364, doi:10.1029/GL017i004p00361.

Wilson, J. C., W. T. Lai, and S. D. Smith (1991), Measurements of condensation nuclei above the jet stream: Evidence for cross jet transport by waves and new particle formation at high altitudes, *J. Geophys. Res.*, *96*, 17,415–17,423, doi:10.1029/91JD01357.

Wyslouzil, B. E., J. H. Seinfeld, R. C. Flagan, and K. Okuyama (1991), Binary nucleation in acid–water systems. II. Sulfuric acid–water and a comparison with methanesulfonic acid–water, *J. Chem. Phys.*, *94*, 6842–6850, doi:10.1063/1.460262.

Zhao, J., O. B. Toon, and R. P. Turco (1995), Origin of condensation nuclei in the springtime polar stratosphere, *J. Geophys. Res.*, *100*, 5215–5227, doi:10.1029/94JD03110.